Dynamic spin susceptibility of superconducting cuprates: A microscopic theory of the magnetic resonance mode

A. A. Vladimirov,[1] D. Ihle,[2] and N. M. Plakida[1,3]
[1]*Joint Institute for Nuclear Research, 141980 Dubna,Russia*
[2]*Institut für Theoretische Physik, Universität Leipzig, D-04109, Leipzig, Germany*
[3]*Max-Planck-Institut für Physik komplexer Systeme, D-01187, Dresden, Germany*
(Received 2 June 2010; published 25 January 2011)

A microscopic theory of the dynamic spin susceptibility (DSS) in the superconducting state within the t-J model is presented. It is based on an exact representation for the DSS obtained by applying the Mori-type projection technique for the relaxation function in terms of Hubbard operators. The static spin susceptibility is evaluated by a sum-rule-conserving generalized mean-field approximation, while the self-energy is calculated in the mode-coupling approximation. The spectrum of spin excitations is studied in a homogeneous phase of the underdoped and optimally doped regions. The DSS reveals a resonance mode (RM) at the antiferromagnetic wave vector $\mathbf{Q} = \pi(1,1)$ at low temperatures due to a strong suppression of the damping of spin excitations. This is explained by an involvement of spin excitations in the decay process in addition to the particle-hole continuum usually considered in random-phase-type approximations. The spin gap in the spin-excitation spectrum at $\mathbf{Q}$ plays a dominant role in limiting the decay in comparison with the superconducting gap, which results in the observation of the RM even above T_c in the underdoped region. A good agreement with inelastic neutron-scattering experiments on the RM in $YBa_2Cu_3O_y$ compounds is found.

DOI: 10.1103/PhysRevB.83.024411 PACS number(s): 74.72.−h, 75.10.−b, 75.40.Gb

I. INTRODUCTION

In the superconducting state the spin-excitation spectrum of high-T_c cuprates is dominated by a sharp magnetic peak at the planar antiferromagnetic (AF) wave vector $\mathbf{Q} = \pi(1,1)$ which is called *the resonance mode* (RM). It was discovered in inelastic neutron scattering (INS) experiments which revealed a suppression of the spectral weight of low-energy spin excitations at low temperatures and its transfer to higher energies, resulting in the RM. There is a vast literature devoted to experimental and theoretical investigations of spin-excitation spectra and the RM in cuprates (a list of references can be found in the reviews[1–5] and in a number of publications, such as, e.g., Refs. 6–9). Here we consider only the main results of these studies relevant for our purposes.

The RM was discovered first in the optimally doped $YBa_2Cu_3O_y$ ($YBCO_y$) crystal at the energy $E_r \approx 41$ meV,[10] but later on, the RM was found in the underdoped $YBCO_y$ crystals, $Bi_2Sr_2CaCu_2O_{8+\delta}$ (Bi-2212) compounds, and other cuprates as well.[2] In particular, the RM was observed in the single-layer cuprate superconductors $Tl_2Ba_2CuO_{6+x}$ (Tl-2201) (Ref. 11) and $HgBa_2CuO_{4+\delta}$ (Hg-1201),[12] and in the electron-doped $Pr_{0.88}LaCe_{0.12}CuO_{4-\delta}$ superconductor.[13] This demonstrates that the RM is a generic feature of the cuprate superconductors and can be related to spin excitations in a single CuO_2 layer. Since the energy of the RM was found to scale with the superconducting temperature, $E_r \approx 5.3 k_B T_c$ in YBCO and Bi-2212 compounds and $E_r \approx 6 k_B T_c$ ($6.8 k_B T_c$) in Tl-2201 (Hg-1201) systems, it has been argued that it might constitute the bosonic excitation mediating superconducting pairing in cuprates, which has motivated an extensive study of the RM phenomenon (see, e.g., Refs. 4,5).

The spin-excitation dispersion close to the RM exhibits a peculiar "hourglasslike" shape with upward and downward dispersions. Whereas the RM energy E_r changes with doping, no essential temperature dependence of E_r and of the upward branch of the dispersion has been found. In the optimal doping region the RM and both dispersion branches are smeared out above T_c. In a strongly underdoped YBCO crystal only the downward branch is suppressed above T_c, whereas the upward dispersion and the RM are observed in the normal pseudogap state. In particular, a well-defined resonance peak at $E_r \approx 33$ meV was found in the $YBCO_{6.5}$ crystal in the oxygen-ordered ortho-II phase with $T_c = 59$ K at hole doping $p = 0.09$ (Refs. 14,15). At low temperature, $T \sim 8$ K, the RM revealed a much higher intensity than in optimally doped crystals, and it was also seen with less intensity even at $T \simeq 1.4 T_c$.

The extensive study of the twin-free $YBCO_{6.6}$ crystal with $T_c = 61$ K at hole doping $p = 0.12$ (Refs. 16,17) revealed a different origin of the upward and downward parts of the spin excitations close to the RM energy $\omega_r = 38.5$ meV. Specifically, the high-energy excitations do not show noticeable changes at the superconducting transition and have the symmetry of the square CuO_2 lattice common to all cuprates. Contrary to this, the low-energy part of the spectrum is qualitatively different in the superconducting and pseudogap states. In Ref. 17 the INS data were fitted by a spectral function of spin excitations in absolute units which was used to calculate the effective spin-fluctuation-mediated pairing interaction and to estimate the superconducting temperature $T_c \sim 170$ K.[18]

An hourglass structure of the spin-excitation spectrum similar to that in YBCO was found in $La_{2-x}Sr_xCuO_4$ (LSCO-x) crystals (see Refs. 19–21). However, no sharp RM was found at $T < T_c$, which may be caused by strong disorder effects produced by Sr doping close to the CuO_2 plane or by dynamically fluctuating stripes. A double-peaked structure was observed in the local susceptibility $\chi''(\omega)$ of the optimally doped LSCO-0.16 crystal[20] with $T_c = 38.5$ K. The lower-energy incommensurate (IC) part of the spectrum

was found below $\omega \sim 20$ meV, which may be explained by electron-hole collective excitations (or fluctuating stripes), whereas the high-energy upward dispersion, peaked at $\omega = 40$–50 meV, can be viewed as overdamped spin-wave-like excitations caused by the residual AF exchange interaction $J \sim 80$ meV. A similar, though less pronounced, double-peaked structure in $\chi''(\omega)$ was found in the underdoped LSCO-0.085 crystal with $T_c = 22$ K in the pseudogap phase.[21]

Generally, the INS experiments suggest the universality of the hourglass structure of spin excitations in cuprates, though with material-dependent details. The high-energy excitations above the RM can be considered as overdamped AF spin waves with the exchange interaction decreasing with doping. Since the characteristic exchange energy, especially at low doping, is quite large, only a weak temperature dependence of the spectrum is observed, resulting from the increase of the damping with temperature that shifts the maximum of the dynamic spin susceptibility (DSS) to a lower energy. The low-energy spin dynamics, which reveals a strong temperature dependence below T_c, may be related to fluctuating stripe phases with a quasi-one-dimensional order of spins and charges or to a nematic (liquid crystal) state as discussed later.

To explain the RM in superconducting cuprates, various theoretical models have been proposed. In a large number of studies the Fermi-liquid model of itinerant electrons was assumed and the DSS was calculated by the random phase approximation (RPA) for the one-band Hubbard model or by taking the RPA susceptibility with the AF superexchange interaction $J(\mathbf{q})$ (see, e.g., Refs. 22–24). In this approach, the RM is considered as a particle-hole-bound state, usually referred to as a spin-1 exciton. The state is formed below the continuum of particle-hole excitations which is gapped at a threshold energy $\omega_c \leqslant 2\Delta(\mathbf{q}^*)$ determined by the superconducting d-wave gap $2\Delta(\mathbf{q}^*)$ at a particular wave vector $\mathbf{q}^*$ on the Fermi surface (FS). In the Fermi-liquid approach, the d-wave symmetry of the gap and the shape of the FS which should cross the AF Brillouin zone are essential in explaining the $\mathbf{q}$ and ω dependence of the DSS and the RM.

More complicated electronic models were also considered, e.g., in Refs. 6,25–28, where an extensive study of magnetic interactions was performed for the extended three-band Hubbard model with large Cu on-site correlation U. Using the slave-boson representation and $1/N$ expansion (N is the spin degeneracy) the spectrum of spin excitations was calculated both for the normal state and for the superconducting d-wave state. It was stressed that a difference of the magnetic neutron scattering in the LSCO and YBCO compounds could be explained by fine details of the band structure.[26,28] To explain the peculiarity of the DSS and the RM in the two-layer YBCO compounds, a bilayer exchange interaction was invoked (see, e.g., Refs. 27,29). Usually the downward IC dispersion is well reproduced by fitting the electron interaction while the intensity of the upward dispersion appears to be too weak. To describe the underdoped regime close to the insulating (and AF) state, where a model of itinerant electrons cannot be justified, a phenomenological spin-fermion model was used (see, e.g., Ref. 4).

The INS study of the slightly overdoped Bi-2212 crystal[30] and of $Y_{1-x}Ca_xB_2Cu_3O_{6+x}$ (Y-CaBCO) compounds[31] seems to support the spin-exciton scenario. In particular, the global momentum shape of the measured magnetic excitations is quantitatively described within the spin-exciton model with parameters inferred from angle-resolved photoemission experiments on Bi-2212 or electronic Raman scattering experiments on Y-CaBCO. However, the temperature dependence of the RM energy was not studied; this should be observed in the spin-exciton model due to the temperature dependence of the superconducting gap.

The strong-correlation limit in the underdoped region in cuprates is often treated within the t-J model suitable for consideration of low-energy spin dynamics. To take into account the projected character of electron operators, the slave-boson technique was used (for a review see Ref. 32). In particular, in Ref. 33 the magnetic excitation spectrum was studied within the t-t'-J model using the mean-field slave-particle theory. The DSS was calculated in the RPA for spinons in the superconducting and spin-gap states. The RM was revealed as the spin-1 exciton below the threshold energy, as in the Fermi-liquid models. A qualitative agreement with INS experiments on YBCO and Bi-2212 compounds was obtained. In Ref. 9, a comprehensive analysis of the DSS within the mean-field slave-boson theory for the bilayer t-J model was performed. A special emphasis was put on the explanation of an anisotropy of the spectrum in the square CuO_2 plane, which was related to a d-wave-shaped FS deformation (dFSD). In the case of a strong dFSD a spontaneous breaking of the orientational symmetry of the FS can occur leading to its orthorhombic deformation (Pomeranchuk instability). The DSS was calculated in the RPA with a renormalized in-plane AF exchange interaction. Within the theory, both the collective RM and its downward dispersion as well as the high-energy excitations with the upward dispersion were obtained. It was also possible to explain the in-plane anisotropy of the DSS observed in INS experiments by the dFSD effect.

However, in the slave-particle theory one has to introduce a local constraint at each lattice site to reduce the enlarged Hilbert space (four states per site) to the physical one of the projected electronic states (three states per site in the t-J model). In the mean-field approximation the local constraint is relaxed and substituted by an averaged one which violates the constraint and leads to uncontrollable results.

A rigorous approach is based on the Hubbard operators (HOs) acting in the correct physical space.[34] In Ref. 35, a special diagram technique for the HOs was developed and used to calculate the DSS. In particular, a generalized RPA was elaborated by summing up different types of bubble diagrams. However, the RM excitation was not considered there. Calculations of the DSS within the HO technique in the conventional RPA in Ref. 36 revealed a sharp RM, caused by the opening of the superconducting gap below T_c, and low-energy collective excitations similar to the results for the Fermi-liquid models.

Let us make a general remark concerning the spin-1 exciton scenario based on a summation of fermion-bubble-type diagrams, as in the conventional RPA. In this scenario, a strong temperature dependence of the RM energy is expected below T_c due to the temperature dependence of the superconducting gap $2\Delta(\mathbf{q}^*)$ and, hence, of the threshold energy ω_c and $E_r < \omega_c$. However, this contradicts the experiments. In theoretical

calculations, usually only the low-temperature limit, $T \ll T_c$, and the $T > T_c$ region are analyzed. It would be important to study a region at $T \leqslant T_c$ to test the spin-1 exciton scenario.

To go beyond a simple RPA in the strong-correlation limit, the Mori projection technique[37] in the equation of motion method for the relaxation function has been used by several groups (see, e.g., Refs. 38–43). In the t-J model, this method allows consideration of the magnetic excitations of localized spins in the undoped case within the AF Heisenberg model and a crossover to the itinerant-electron spin excitations in the overdoped region. These studies and, in particular, the DSS calculation and the RM analysis in the superconducting state will be discussed later and compared with our results. In Refs. 44 and 45, we have formulated a rigorous theory of the DSS in the normal state within the projection operator method for the relaxation function in terms of the HOs. The results obtained, both for the static properties (like the staggered magnetization at $T = 0$, the uniform static susceptibility, and the AF correlation length) and for the DSS [e.g., the (ω/T)-scaling behavior of the local DSS] have shown a good agreement with available cluster calculations and neutron-scattering data. In particular, it was shown that the kinematical interaction resulting from the HO commutation relations plays an essential role and gives the major contribution to the damping of spin excitations induced by the hopping term t.

In this respect, we mention a calculation of the DSS using the Mori projection technique for the t-J model.[46] In this study, the projected character of electron operators was neglected by replacing them with the conventional Fermi operators. As a result, the kinematical interaction induced by a large hopping term $t \simeq 3J$ was disregarded and only the exchange interaction J was considered. The resulting Mori memory function was represented as a sum of two contributions, one determined by electrons in the conventional RPA and the second given by the spin-spin scattering proprotional to J^2. Although the upward and downward dispersions of the spin-excitation spectrum and the RM below T_c were reproduced, ignoring the hopping term contribution to the memory function can give only a qualitative description.

The discovery of the static IC charge- and spin-density waves (CDW and SDW), referred to as stripes, in the metallic phase of $La_{2-x}Ba_xCuO_4$ (LBCO-x) and LSCO compounds has attracted much attention in recent years and was used in the explanation of the IC spin-excitation spectrum in hole-doped cuprates (for reviews see Refs. 47–49). In particular, in the stripe phase of the LBCO-0.125 compound an INS study at $T = 12$ K ($> T_c$) revealed high-energy spin excitations at $\omega > 40$ meV and a low-energy branch similar to spin waves in the two-leg-ladder spin model.[50] Various stripe models have been proposed to describe the experimental data. In particular, spin-only models for the bond-centered stripe with long-range magnetic order in Ref. 51 and a two-dimensional (2D) model of coupled two-leg spin ladders in Ref. 52 were proposed, which fitted the experimental data quite well. In Ref. 53, both bond- and site-centered stripes were considered within the time-dependent Gutzwiller approximation for the Hubbard model. Static stripe spin and charge order coexisting with the d-wave superconductivity was studied within an extended Hubbard model in the mean-field approximation and RPA for the DSS in Ref. 54. Using quantum Monte Carlo simulations a detailed study of magnetic excitations was performed for coupled spin ladders.[55] Magnetic ordering both perpendicular and parallel to the stripe direction was found in an array of antiferromagnetically coupled doped and undoped two-leg ladders.[56]

However, the static stripes have not been detected in moderately doped YBCO crystals, where only dynamically fluctuating stripes can be suggested (see, e.g., Refs. 8,14–16,57). Moreover, instead of a rigid stripe array proposed in Ref. 58, 2D character of the IC spin fluctuations was observed in untwinned $YBCO_{6+x}$ crystals with $x = 0.6$ and 0.85.[57] The IC peaks exhibiting in-plane anisotropy were explained as a result of a possible liquid-crystalline stripe phase or a nematic state. Therefore, although the inhomogeneous stripe picture can be applied for LSCO and LBCO systems, it seems to be not a universal origin of the hourglass spin-excitation dispersion and the RM in cuprate superconductors. Inhomogeneous phases of cuprates related to fluctuating stripes with a quasi-one-dimensional order of spins and charges or to a liquid-crystal state may be important only in the explanation of the low-energy collective spin fluctuations.

To clarify some of the open problems in describing the RM phenomenon, such as the appearance of the RM above T_c and its weak temperature dependence, in the present paper we extend our microscopic theory (Refs. 44 and 45) to the superconducting state. Although our general formulation for the DSS is similar to the original Mori memory function approach used in other publications, as in Ref. 38, in the previous studies of the t-J model only the bubble-type diagrams similar to the RPA were considered, which ignores the important role of spin excitations in the decay process. The energy gap at the AF wave vector $\mathbf{Q}$ of the order of the RM energy E_r in the spin-excitation spectrum strongly reduces the damping at low temperatures, $T \ll E_r \simeq 5\,k_B T_c$, which results in the emergence of a sharp peak in the spectral function. In the low-doping region, where the damping is extremely small, the RM is found even above T_c. In the overdoped region, at hole concentration $\delta \sim 0.2$ and high T_c, the spin-excitation damping becomes large and the opening of the superconducting gap enhances the intensity of the RM,so that it becomes observable only below T_c. So, as compared with the spin-exciton scenario, we propose an alternative explanation of the RM and the upper branch of the dispersion: that they are driven by the spin gap at $\mathbf{Q}$ instead of the superconducting gap 2Δ. A good agreement of our results for the temperature and doping dependence of the spin-excitation spectrum and the RM with INS experiments provides strong support for the proposed theory. We have not found a lower branch of the hourglass spectrum, which may be related to inhomogeneous states in the CuO_2 plane neglected in our analysis.

In the next section we present the basic formulas for the DSS and the self-energy, which are a generalization of our theory in Ref. 45 to the superconducting state. Numerical results for the spin-excitation spectra are given in Sec. III, where the temperature and doping dependence of the damping and the RM are discussed. The conclusion is given in Sec. IV. Details

of the calculations within the mode-coupling approximation (MCA) are presented in the Appendix.

II. RELAXATION-FUNCTION THEORY

A. Dynamic spin susceptibility

It is convenient to consider the t-J model in the Hubbard operator representation

$$H = -\sum_{i\neq j,\sigma} t_{ij} X_i^{\sigma 0} X_j^{0\sigma} - \mu \sum_{i\sigma} X_i^{\sigma\sigma} + \frac{1}{4}\sum_{i\neq j,\sigma} J_{ij}\left(X_i^{\sigma\bar{\sigma}} X_j^{\bar{\sigma}\sigma} - X_i^{\sigma\sigma} X_j^{\bar{\sigma}\bar{\sigma}}\right), \quad (1)$$

where t_{ij} is the hopping integral and J_{ij} is the exchange interaction. The Hubbard operators $X_i^{\alpha\beta} = |i,\alpha\rangle\langle i,\beta|$ describe transitions between three possible states at a site i on a square lattice: an empty state $|i,\alpha\rangle = |i,0\rangle$ and a singly occupied state $|i,\alpha\rangle = |i,\sigma\rangle$ with spin $\sigma = \pm(1/2)$ ($\bar{\sigma} = -\sigma$). The number and spin operators in terms of the Hubbard operators read

$$N_i = \sum_\sigma X_i^{\sigma\sigma}, \quad S_i^\sigma = X_i^{\sigma\bar{\sigma}}, \quad S_i^z = \sum_\sigma \sigma X_i^{\sigma\sigma}. \quad (2)$$

The Hubbard operators obey the completeness relation $X_i^{00} + \sum_\sigma X_i^{\sigma\sigma} = 1$ which preserves rigorously, contrary to the slave-boson approach, the constraint of no double occupancy of any lattice site. The Hubbard operators have the commutation relations $[X_i^{\alpha\beta}, X_j^{\gamma\delta}]_\pm = \delta_{ij}(\delta_{\beta\gamma} X_i^{\alpha\delta} \pm \delta_{\delta\alpha} X_i^{\gamma\beta})$ which results in a *kinematical interaction*. Here, the upper sign pertains to Fermi-type operators like $X_i^{0\sigma}$ changing the number of electrons, and the lower sign pertains to Bose-type operators, such as the number operator or the spin operators, Eq. (2). The chemical potential μ is determined from the equation for the average electron density $n = \langle N_i\rangle = 1 - \delta$, where $\delta = \langle X_i^{00}\rangle$ is the hole concentration.

In Ref. 44, applying the Mori-type projection technique,[37] elaborated for the relaxation function, we have derived an exact representation for the DSS $\chi(\mathbf{q},\omega)$ related to the retarded commutator Green function (GF) (see Ref. 59),

$$\chi(\mathbf{q},\omega) = -\langle\langle S_\mathbf{q}^+ | S_{-\mathbf{q}}^-\rangle\rangle_\omega = \frac{m(\mathbf{q})}{\omega_\mathbf{q}^2 + \omega\,\Sigma(\mathbf{q},\omega) - \omega^2}, \quad (3)$$

where $m(\mathbf{q}) = \langle[i\dot{S}_\mathbf{q}^+, S_{-\mathbf{q}}^-]\rangle = \langle[[S_\mathbf{q}^+, H], S_{-\mathbf{q}}^-]\rangle$, and $\omega_\mathbf{q}$ is the spin-excitation spectrum in a generalized mean-field approximation (GMFA). The self-energy is given by the many-particle Kubo-Mori relaxation function

$$\Sigma(\mathbf{q},\omega) = [1/m(\mathbf{q})]\,\big((-\ddot{S}_\mathbf{q}^+ | -\ddot{S}_{-\mathbf{q}}^-)\big)_\omega^{(\mathrm{proper})}, \quad (4)$$

where $-\ddot{S}_\mathbf{q}^\pm = [[S_\mathbf{q}^\pm, H], H]$ (for details see Ref. 44). The Kubo-Mori relaxation function and the scalar product are defined as (see, e.g., Ref. 60)

$$\big((A|B)\big)_\omega = -i\int_0^\infty dt e^{i\omega t}\big(A(t), B\big) \quad (5)$$

and

$$\big(A(t), B\big) = \int_0^\beta d\lambda \langle A(t - i\lambda)B\rangle, \quad \beta = 1/k_\mathrm{B}T, \quad (6)$$

respectively. The "proper" part of the relaxation function (4) does not contain parts connected by a single zero-order relaxation function which corresponds to the projected time evolution in the original Mori projection technique.[37] The spin-excitation spectrum is given by the spectral function defined by the imaginary part of the DSS (3),

$$\chi''(\mathbf{q},\omega) = \frac{-\omega\,\Sigma''(\mathbf{q},\omega)\,m(\mathbf{q})}{\left[\omega^2 - \omega_\mathbf{q}^2 - \omega\,\Sigma'(\mathbf{q},\omega)\right]^2 + [\omega\,\Sigma''(\mathbf{q},\omega)]^2}, \quad (7)$$

where $\Sigma(\mathbf{q},\omega + i0^+) = \Sigma'(\mathbf{q},\omega) + i\Sigma''(\mathbf{q},\omega)$, and $\Sigma'(\mathbf{q},\omega) = -\Sigma'(\mathbf{q},-\omega)$ and $\Sigma''(\mathbf{q},\omega) = \Sigma''(\mathbf{q},-\omega) < 0$ are the real and imaginary parts of the self-energy, respectively.

B. Static susceptibility

The general representation of the DSS (3) determines the static susceptibility $\chi_\mathbf{q} = \chi(\mathbf{q},0)$ by the equation

$$\chi_\mathbf{q} = (S_\mathbf{q}^+, S_{-\mathbf{q}}^-) = m(\mathbf{q})/\omega_\mathbf{q}^2. \quad (8)$$

To calculate the spin-excitation spectrum $\omega_\mathbf{q}$ the equality

$$m(\mathbf{q}) = (-\ddot{S}_\mathbf{q}^+, S_{-\mathbf{q}}^-) = \omega_\mathbf{q}^2\,(S_\mathbf{q}^+, S_{-\mathbf{q}}^-) \quad (9)$$

is used, where the correlation function $(-\ddot{S}_\mathbf{q}^+, S_{-\mathbf{q}}^-)$ is evaluated in the GMFA by a decoupling procedure in the site representation as described in Ref. 45. This procedure is equivalent to the MCA for the two-time correlation functions. This results in the spin-excitation spectrum

$$\omega_\mathbf{q}^2 = 8t^2\lambda_1(1-\gamma_\mathbf{q})(1 - n - F_{2,0} - 2F_{1,1}) + 4J^2(1-\gamma_\mathbf{q})\Big[\lambda_2\frac{n}{2} - \alpha_1 C_{1,0}(4\gamma_\mathbf{q} + 1) + \alpha_2(2C_{1,1} + C_{2,0})\Big], \quad (10)$$

where t and J are the hopping integral and the exchange interaction for the nearest neighbors, respectively, and $\gamma_\mathbf{q} = (1/2)(\cos q_x + \cos q_y)$ (we take the lattice spacing a to be unity). The static electron and spin correlation functions are defined as

$$F_{n,m} \equiv F_\mathbf{R} = \left\langle X_\mathbf{0}^{\sigma 0}\, X_\mathbf{R}^{0\sigma}\right\rangle = \frac{1}{N}\sum_\mathbf{q} F_\mathbf{q} e^{i\mathbf{qR}}, \quad (11)$$

$$C_{n,m} \equiv C_\mathbf{R} = \langle S_\mathbf{0}^-\, S_\mathbf{R}^+\rangle = \frac{1}{N}\sum_\mathbf{q} C_\mathbf{q} e^{i\mathbf{qR}}, \quad (12)$$

where $\mathbf{R} = n\mathbf{a}_x + m\mathbf{a}_y$. The GMFA spectrum (10) is calculated self-consistently by using the GMFA approximation for the static correlation function (12),

$$C_\mathbf{q} = \frac{m(\mathbf{q})}{2\,\omega_\mathbf{q}}\coth\frac{\beta\,\omega_\mathbf{q}}{2}. \quad (13)$$

The decoupling parameters α_1,α_2 and λ_1,λ_2 in Eq. (10) take into account the vertex renormalization for the spin-spin and electron-spin interaction, respectively, as explained in Ref. 45. In particular, the parameters α_1,α_2 are evaluated from the results for the Heisenberg model at $\delta = 0$ and are kept fixed for $\delta \neq 0$. The parameters λ_1,λ_2 are calculated from the sum rule $C_{0,0} = \langle S_0^+ S_0^-\rangle = (1/2)(1-\delta)$ with a fixed ratio $\lambda_1/\lambda_2 = 0.378$. In the superconducting state, the electron

correlation function $F_{\mathbf{R}}$ is calculated by the spectral function for electrons in the superconducting state [see Eq. (22)]. The variation of the parameters λ_1,λ_2 below the superconducting transition is negligibly small and has essentially no influence on the spectrum $\omega_{\mathbf{q}}$.

The direct calculation of $m(\mathbf{q})$ yields

$$m(\mathbf{q}) = -8\,(1-\gamma_{\mathbf{q}})\,[t\,F_{1,0} + J\,C_{1,0}]. \tag{14}$$

Thus, the static susceptibility (8) is explicitly determined by Eqs. (10) and (14).

C. Self-energy

In what follows, we consider the t-J model at a finite hole doping $\delta > 0.05$ when, as discussed in Ref. 45, the largest contribution to the self-energy (4) is $\Sigma_t(\mathbf{q},\omega)$ coming from the spin-electron scattering. It is determined by the hopping term H_t in the t-J model according to the equation for the spin-density operators: $-\ddot{S}^{\pm}_{\mathbf{q}} = [\,[S^{\pm}_{\mathbf{q}}, H_t\,], H_t]$. As described in the Appendix, in the MCA this contribution reads

$$\begin{aligned}\Sigma''_t(\mathbf{q},\omega) = &-\frac{\pi(2t)^4(e^{\beta\omega}-1)}{m(\mathbf{q})\,\omega}\\ &\times\int\!\!\int\!\!\int_{-\infty}^{\infty} d\omega_1 d\omega_2 d\omega_3 \frac{1}{N^2}\sum_{\mathbf{q}_1,\mathbf{q}_2} N(\omega_2)\\ &\times[1-n(\omega_1)]n(\omega_3)\delta(\omega+\omega_1-\omega_2-\omega_3)B_{\mathbf{q}_2}(\omega_2)\\ &\times\Big[\big(\Lambda^2_{\mathbf{q}_1,\mathbf{q}_2,\mathbf{q}_3}+\Lambda^2_{\mathbf{q}_3,\mathbf{q}_2,\mathbf{q}_1}\big)\,A^N_{\mathbf{q}_1}(\omega_1)\,A^N_{\mathbf{q}_3}(\omega_3)\\ &-2\Lambda_{\mathbf{q}_1,\mathbf{q}_2,\mathbf{q}_3}\Lambda_{\mathbf{q}_3,\mathbf{q}_2,\mathbf{q}_1}\,A^S_{\mathbf{q}_1\sigma}(\omega_1)\,A^S_{\mathbf{q}_3\sigma}(\omega_3)\Big],\end{aligned} \tag{15}$$

where $\mathbf{q}_3 = \mathbf{q}-\mathbf{q}_1-\mathbf{q}_2$. The Fermi and Bose functions are denoted by $n(\omega) = (e^{\beta\omega}+1)^{-1}$ and $N(\omega) = (e^{\beta\omega}-1)^{-1}$. The vertex function $\Lambda_{\mathbf{q}_1,\mathbf{q}_2,\mathbf{q}_3}$ is defined by Eq. (A5). Here we introduced the spectral functions

$$A^N_{\mathbf{q}}(\omega) = -(1/\pi)\mathrm{Im}\big\langle\big\langle X^{0\sigma}_{\mathbf{q}}\,\big|\,X^{\sigma 0}_{\mathbf{q}}\big\rangle\big\rangle_{\omega}, \tag{16}$$

$$A^S_{\mathbf{q}\sigma}(\omega) = -(1/\pi)\mathrm{Im}\big\langle\big\langle X^{0\sigma}_{\mathbf{q}}\,\big|\,X^{0\bar{\sigma}}_{-\mathbf{q}}\big\rangle\big\rangle_{\omega}, \tag{17}$$

$$B_{\mathbf{q}}(\omega) = (1/\pi)\,\chi''(\mathbf{q},\omega), \tag{18}$$

where $A^{N,S}_{\mathbf{q}}(\omega)$ are determined by the retarded anticommutator GFs for electrons (see Ref. 59). In comparison with the expression for the self-energy in the normal state considered in Ref 45, in Eq. (15) there is a contribution proportional to the anomalous GF $\langle\langle X^{0\sigma}_{\mathbf{q}}|X^{0\bar{\sigma}}_{-\mathbf{q}}\rangle\rangle_{\omega}$ which is nonzero in the superconducting state only.

It should be emphasized that the self-energy (15) is determined by the decay of a spin excitation with the energy ω and wave vector $\mathbf{q}$ into three excitations: a particle-hole pair and a spin excitation. This process is controlled by the energy and momentum conservation laws $\omega = (\omega_3-\omega_1)+\omega_2$ and $\mathbf{q} = \mathbf{q}_1+\mathbf{q}_2+\mathbf{q}_3$, respectively. In previous studies of the t-J model the contribution of the additional spin excitation has been neglected (see, e.g., Ref. 36) or approximated by static or mean-field-type expressions (see, e.g., Refs. 38 and 42). That is, in these approximations the spin-excitation contribution was "decoupled" from the particle-hole pair. We can derive the particle-hole bubble approximation from Eq. (15), if we ignore the spin-energy contribution ω_2 in comparison with the electron-hole pair energy, or, equivalently, if in the MCA, Eqs. (A6) and (A7), the time-dependent spin-correlation function is approximated by its static value: $\langle S^-_{-\mathbf{q}}S^+_{\mathbf{q}}(t)\rangle \simeq \langle S^-_{-\mathbf{q}}S^+_{\mathbf{q}}\rangle = C_{\mathbf{q}}$. Moreover, excluding the spin-excitation wave vector $\mathbf{q}_2$ from the wave-vector conservation law, we have $\mathbf{q} = \mathbf{q}_1+\mathbf{q}_3$. As a result of these approximations in Eq. (15), we obtain the self-energy in the form of the particle-hole bubble approximation:

$$\begin{aligned}\widetilde{\Sigma}''_t(\mathbf{q},\omega) = &-\frac{\pi(2t)^4}{m(\mathbf{q})\,\omega}\int_{-\infty}^{\infty} d\omega_1[n(\omega_1)-n(\omega_1+\omega)]\\ &\times\frac{1}{N}\sum_{\mathbf{q}_1}\big[\widetilde{\Lambda}^N_{\mathbf{q}_1,\mathbf{q}-\mathbf{q}_1}\,A^N_{\mathbf{q}_1}(\omega_1)\,A^N_{\mathbf{q}-\mathbf{q}_1}(\omega_1+\omega)\\ &-\widetilde{\Lambda}^S_{\mathbf{q}_1,\mathbf{q}-\mathbf{q}_1}\,A^S_{\mathbf{q}_1\sigma}(\omega_1)\,A^S_{\mathbf{q}-\mathbf{q}_1\sigma}(\omega_1+\omega)\big],\end{aligned} \tag{19}$$

where the vertices averaged over the spin-excitation wave vector $\mathbf{q}_2$ are introduced,

$$\widetilde{\Lambda}^N_{\mathbf{q}_1,\mathbf{q}_3} = \frac{1}{N}\sum_{\mathbf{q}_2} C_{\mathbf{q}_2}\big[\Lambda^2_{\mathbf{q}_1,\mathbf{q}_2,\mathbf{q}_3}+\Lambda^2_{\mathbf{q}_3,\mathbf{q}_2,\mathbf{q}_1}\big], \tag{20}$$

$$\widetilde{\Lambda}^S_{\mathbf{q}_1,\mathbf{q}_3} = \frac{2}{N}\sum_{\mathbf{q}_2} C_{\mathbf{q}_2}\Lambda_{\mathbf{q}_1,\mathbf{q}_2,\mathbf{q}_3}\Lambda_{\mathbf{q}_3,\mathbf{q}_2,\mathbf{q}_1}. \tag{21}$$

In the approximation (19) only the opening of a superconducting gap in the particle-hole excitation can suppress the damping of spin excitations due to the decay into particle-hole pairs which may result in the RM. Below we discuss in more detail why a particle-hole bubble approximation for the self-energy, Eq. (19), leads to a different behavior of the spin-excitation damping in comparison with the results obtained for the full self-energy (15).

III. RESULTS AND DISCUSSION

A. Self-energy approximation

In the calculation of the self-energy (15) we adopt the mean-field approximation (MFA) for the electron spectral functions (16) and (17), which in the superconducting state can be written as

$$A^N_{\mathbf{q}}(\omega) = Q\sum_{\omega_1=\pm E_{\mathbf{q}}}\frac{\omega_1+\varepsilon_{\mathbf{q}}}{2\omega_1}\delta(\omega-\omega_1), \tag{22}$$

$$A^S_{\mathbf{q}\sigma}(\omega) = Q\sum_{\omega_1=\pm E_{\mathbf{q}}}\frac{\Delta_{\mathbf{q}\sigma}}{2\omega_1}\delta(\omega-\omega_1). \tag{23}$$

Here $Q = 1-n/2$ is the Hubbard weighting factor and the superconducting gap function $\Delta_{\mathbf{q}\sigma} = (\mathrm{sgn}\sigma)\,\Delta_{\mathbf{q}}$. In the electron spectrum $\varepsilon_{\mathbf{q}}$ we take into account only the nearest-neighbor hopping t and consider the energy dispersion in the Hubbard-I approximation: $\varepsilon_{\mathbf{q}} = -4tQ\gamma_{\mathbf{q}}-\mu$. The spectrum of quasiparticles in the superconducting state is given by the conventional formula $E_{\mathbf{q}} = \sqrt{\varepsilon^2_{\mathbf{q}}+\Delta^2_{\mathbf{q}}}$. For the spin-excitation spectral function (18) we take the form

$$B_{\mathbf{q}}(\omega) = m(\mathbf{q})\sum_{\omega_1=\pm\widetilde{\omega}_{\mathbf{q}}}\frac{1}{2\omega_1}\delta(\omega-\omega_1), \tag{24}$$

where the spectrum of spin excitations $\widetilde{\omega}_{\mathbf{q}}$ is determined by the pole of the DSS, $\widetilde{\omega}_{\mathbf{q}} = [\omega^2_{\mathbf{q}}+\widetilde{\omega}_{\mathbf{q}}\,\Sigma'(\mathbf{q},\widetilde{\omega}_{\mathbf{q}})]^{1/2}$. Here, the real part of the self-energy $\Sigma'(\mathbf{q},\omega)$ is calculated perturbationally by taking the spectral function (24) with the GMFA spectrum

$\omega_1 = \pm\omega_{\mathbf{q}}$. Using these spectral functions, after integration over the energies in Eq. (15) we write the imaginary part of the self-energy in the following form convenient for calculation in the limit $T \to 0$:

$$\Sigma_t''(\mathbf{q},\omega) = \frac{\pi(2t)^4}{\omega m(\mathbf{q})}\frac{Q^2}{N^2}\sum_{\mathbf{q}_1,\mathbf{q}_2}\sum_{\omega_1=\pm E_{\mathbf{q}_1}}\sum_{\omega_2=\pm\widetilde{\omega}_{\mathbf{q}_2}}\sum_{\omega_3=\pm E_{\mathbf{q}_3}} m(\mathbf{q}_2) \times\frac{N(\omega_2)n(-\omega_1)n(\omega_3)+N(-\omega_2)n(\omega_1)n(-\omega_3)}{8\omega_1\omega_2\omega_3} \times\Big[\big(\Lambda^2_{\mathbf{q}_1,\mathbf{q}_2,\mathbf{q}_3}+\Lambda^2_{\mathbf{q}_3,\mathbf{q}_2,\mathbf{q}_1}\big)(\omega_1+\varepsilon_{\mathbf{q}_1})(\omega_3+\varepsilon_{\mathbf{q}_3}) - 2\Lambda_{\mathbf{q}_1,\mathbf{q}_2,\mathbf{q}_3}\Lambda_{\mathbf{q}_3,\mathbf{q}_2,\mathbf{q}_1}\Delta_{\mathbf{q}_1}\Delta_{\mathbf{q}_3}\Big] \times\delta(\omega+\omega_1-\omega_2-\omega_3). \quad (25)$$

Similar calculations for the self-energy (19) in the particle-hole bubble approximation yield

$$\widetilde{\Sigma}_t''(\mathbf{q},\omega) = -\frac{\pi(2t)^4}{m(\mathbf{q})\omega}\frac{Q^2}{N}\sum_{\mathbf{q}_1}\sum_{\omega_1=\pm E_{\mathbf{q}_1}}\sum_{\omega_2=\pm E_{\mathbf{q}-\mathbf{q}_1}} \times\frac{n(\omega_1)-n(\omega_2)}{4\omega_1\omega_2}\Big[\widetilde{\Lambda}^N_{\mathbf{q}_1,\mathbf{q}-\mathbf{q}_1}(\omega_1+\varepsilon_{\mathbf{q}_1})(\omega_2+\varepsilon_{\mathbf{q}-\mathbf{q}_1}) - \widetilde{\Lambda}^S_{\mathbf{q}_1,\mathbf{q}-\mathbf{q}_1}\Delta_{\mathbf{q}_1}\Delta_{\mathbf{q}-\mathbf{q}_1}\Big]\delta(\omega+\omega_1-\omega_2). \quad (26)$$

We consider both the d-wave and s-wave symmetry of the superconducting gap, which we write as $\Delta^{(d)}_{\mathbf{q}} = (\Delta/2)(\cos q_x - \cos q_y)$ and $\Delta^{(s)} = \Delta$ with the temperature-dependent amplitude $\Delta(T)$. In numerical calculations we assume that $\Delta(T)$ follows the conventional Bardeen-Cooper-Schrieffer (BCS) theory. In particular, $\Delta(T)/k_{\mathrm{B}}T_{\mathrm{c}} = 1.76, 1.72, 1.6, 1.24$ for $T/T_{\mathrm{c}} = 0, 0.4, 0.6, 0.8$, respectively. By taking, instead of the BCS ratio $2\Delta_0/k_{\mathrm{B}}T_{\mathrm{c}} = 3.52$, $\Delta_0 = \Delta(T=0)$, the ratio $2\Delta_0/k_{\mathrm{B}}T_{\mathrm{c}} = 4.3$ for a pure d-wave superconductor (see, e.g., Ref. 61), we have found that the results do not change noticeably, i.e., by less than 5% at $T = 0$ and even less at finite temperatures. We mainly consider two doping values, $\delta = 0.2$, which is larger than optimal doping, and $\delta = 0.09$ for the underdoped case. For $\delta = 0.2$ we fix the superconducting transition temperature as $k_{\mathrm{B}}T_{\mathrm{c}} = 0.025t$, while for $\delta = 0.09$ we take $k_{\mathrm{B}}T_{\mathrm{c}} = 0.016t$. For the hopping parameter $t = 0.313$ eV these values are close to $T_{\mathrm{c}} = 91$ K in the nearly optimally doped $YBCO_{6.92}$ single crystal in Ref. 1 and $T_{\mathrm{c}} = 59$ K in the underdoped ($\delta = 0.09$) $YBCO_{6.5}$ crystal studied in Ref. 14. We take the exchange interaction $J = 0.3t$ and measure all energies in units of t.

B. Spin-excitation damping

To elucidate the role of spin excitations in the damping and their relevance to the shape of the spectral function Eq. (7), we consider the temperature dependence of the spin-excitation damping at the AF wave vector $\Gamma(\mathbf{Q},\omega) = -(1/2)\,\Sigma_t''(\mathbf{Q},\omega)$. Figure 1 shows the damping for $\delta = 0.2$ at various temperatures in the case of the d-wave (a) and s-wave (b) pairing. The difference of the damping appears only at low ω and T. In particular, the damping for the s-wave gap at $T = 0$ disappears at $\omega < 2\Delta_0 \simeq 4k_{\mathrm{B}}T_{\mathrm{c}} = 0.1t$, while for the d-wave gap it vanishes at $\omega \simeq \Delta_0 \simeq 0.05t$. A weak damping was obtained also for the normal state shown in Fig. 1(c) when the contribution from the superconducting gap functions in the self-energy $\Sigma_t''(\mathbf{Q},\omega)$, Eq. (25), is omitted. The similar smooth variation of the damping with energy in all three cases below T_{c}, contrary to the steplike dependence obtained in the particle-hole bubble approximation (see below), demonstrates that the superconducting gap plays a minor role in suppressing the damping, and the gap $\widetilde{\omega}_{\mathbf{Q}}$ in the spin-excitation spectrum is responsible for such peculiar behavior.

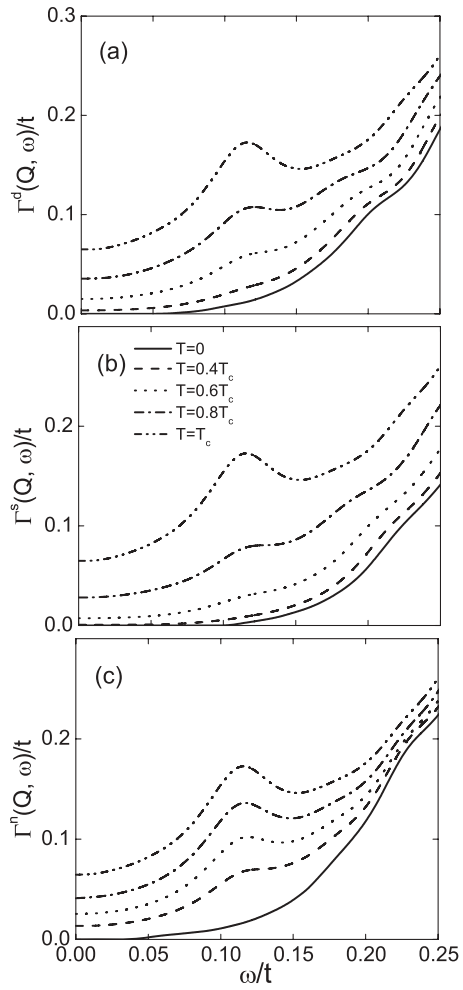

FIG. 1. Spin-excitation damping $\Gamma(\mathbf{Q},\omega)$ for $\delta = 0.2$ at $T \leqslant T_{\mathrm{c}}$ for (a) the d-wave and (b) the s-wave pairing, and (c) in the normal state.

For lower doping, the damping becomes an order of magnitude weaker, as shown in Fig. 2 at $\delta = 0.09$, even above T_{c} ($T = 1.4T_{\mathrm{c}}$). For comparison with results obtained in the fermion-bubble approximation, we calculate the damping also for a more general electron dispersion, $\varepsilon_{\mathbf{q}} = -4t\,\gamma_{\mathbf{q}} + 4t'\,\gamma'_{\mathbf{q}} - 4t''\,\gamma''_{\mathbf{q}} - \mu$, taking into account hopping between next- and third-nearest neighbors, t' and t'', respectively, where $\gamma'_{\mathbf{q}} = \cos q_x \cos q_y$ and $\gamma''_{\mathbf{q}} = (1/2)(\cos 2q_x + \cos 2q_y)$. In Fig. 2 the damping at $T = 0$ for the parameters $t'/t = 0.37$ and $t''/t = 0.1$, proposed in Ref. 18 for the electron dispersion in the antibonding band in $YBCO_{6.6}$, is shown by the dashed line. The difference between the damping calculated for the electron dispersion $\varepsilon_{\mathbf{q}} = -4t\,Q\,\gamma_{\mathbf{q}} - \mu$ in Eqs. (22) and (23) and the more general one with nonzero parameters t' and t'' is negligible. This proves that the shape of the FS and the electron dispersion are unessential factors in our theory. To

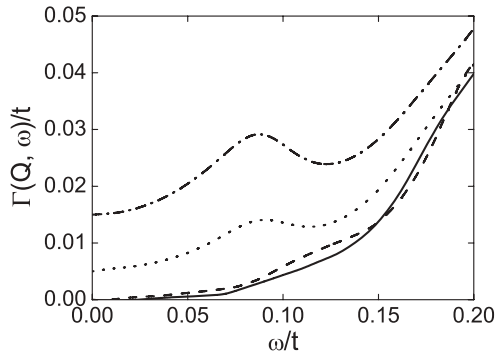

FIG. 2. Spin-excitation damping $\Gamma(\mathbf{Q},\omega)$ for $\delta = 0.09$ for the d-wave pairing at $T = 0$ (solid line), $T = T_c$ (dotted line), and $T = 1.4T_c$ (dash-dotted line). The damping at $T = 0$ for the electron dispersion with $t'/t = 0.37$ and $t''/t = 0.1$ is shown by the dashed line.

describe the electron-doped cuprates within the t-J model, we should change the signs of the hopping parameters t_{ij} in Eq. (1), in particular, $-t \to t > 0$. This replacement does not change the obtained results and, therefore, the theory can be also applied to the electron-doped cuprates with a proper fit of model parameters.

Sometimes, the RM observed above T_c in the underdoped cuprates is related to a pseudogap in the electronic spectrum (see, e.g., Ref. 4). We propose another explanation: The RM above T_c is the result of the gapped spin excitations in the self-energy (25) leading to a very weak damping in the underdoped region, which is outlined in more detail below. This explanation is supported by studies of the spin-excitation damping $\Gamma_{\mathbf{q}} = -(1/2)\,\Sigma_t''(\mathbf{q},\omega = \widetilde{\omega}_{\mathbf{q}})$ at $T = 0$ shown in Fig. 3. The small difference between the damping in the

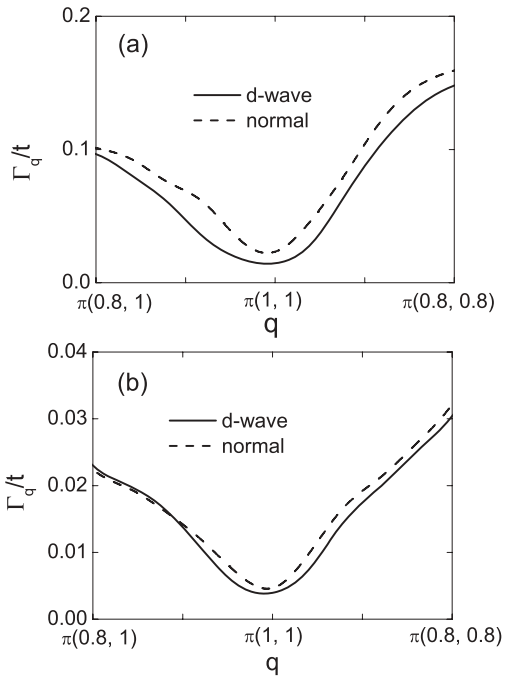

FIG. 3. Spin-excitation damping $\Gamma_{\mathbf{q}}$ for (a) $\delta = 0.2$ and (b) $\delta = 0.09$ at $T = 0$ for the d-wave pairing (solid line) and in the normal state (dashed line).

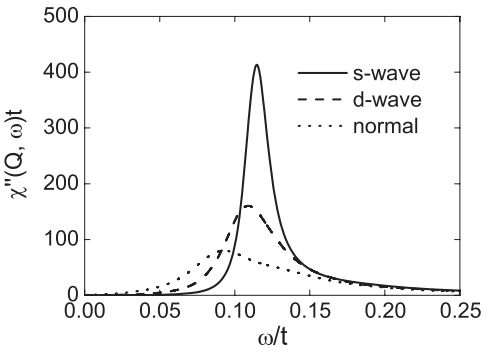

FIG. 4. Spectral function $\chi''(\mathbf{Q},\omega)$ for the d-wave and s-wave pairing in comparison with the normal state at $T = 0.4T_c$ for $\delta = 0.2$.

d-wave superconducting state and the normal state observed for the full self-energy, Eq. (25) confirms that the superconducting gap does not play an essential role in suppressing the damping $\Gamma_{\mathbf{Q}}$, in particular in the underdoped region. At the same time, the sharp increase of $\Gamma_{\mathbf{q}}$ away from the AF wave vector $\mathbf{Q}$ explains the resonance character of spin excitations at $\mathbf{Q}$.

Although the damping in Fig. 1 looks similar, the spectral functions shown in Fig. 4 for $\delta = 0.2$ at $T = 0.4T_c$ reveal a strong enhancement of the intensity of the RM in the superconducting state. In comparison to the normal state, where the contribution from the superconducting gap is omitted, the peak intensity is about two (five) times larger for the d- (s-) wave symmetry of the gap.

Quite a different behavior of the damping and the spectral function is obtained for the reduced self-energy, Eq. (26), with a contribution only from a particle-hole bubble. Figure 5 shows our results for the spectral function $\chi''(\mathbf{q},\omega)$ and for the damping $\Gamma(\mathbf{Q},\omega)$. To compare these functions with those calculated in Ref. 38, we adopt the electron dispersion used in Ref. 38, $\varepsilon_{\mathbf{q}}^{\text{eff}} = -4\,t_{\text{eff}}\gamma_{\mathbf{q}} - 4\,t'_{\text{eff}}\cos q_x \cos q_y$ with $t_{\text{eff}} = 0.3t$ and $t'_{\text{eff}} = -0.1t$, and take the gap parameter $\Delta_0 = 0.1t$. The obtained results are quite close to those shown in Fig. 1 of Ref. 38 [where $\chi''_{zz}(\mathbf{q},\omega) = (1/2)\chi''(\mathbf{q},\omega)$ is plotted]. At $T = 0$, we observe a much narrower RM, but with a lower intensity in comparison with the RM calculated with the full self-energy, Eq. (25), as shown in Fig. 6. The energy E_r of the RM shown in Fig. 5(a) noticeably decreases with increasing temperature, in contrast to the negligible shift of the RM shown in Fig. 6 for $T = 0.4T_c$. This comparison demonstrates that in the particle-hole bubble approximation the superconducting gap plays a crucial role in the occurrence of the RM with $E_r(T) < 2\Delta(T)$, while in the full self-energy (25) the superconducting gap and details of the electron dispersion are less important. In particular, for the underdoped case $\delta = 0.09$ we have not found visible changes of the damping function shown in Fig. 2 for the electron dispersion with $t' = 0$ and $t' = -0.1t$. For the reduced self-energy, Eq. (26), the damping vanishes for both types of dispersion in the underdoped region, and in order to obtain a finite damping at $\delta = 0.1$ in Ref. 38 (see Fig. 2), the authors have to use the electron density of states in the damping function [see their Eq. (20)] instead of the $\mathbf{q}$-dependent electron spectral functions.

This difference can be explained as follows. Whereas in the particle-hole bubble approximation given by Eq. (26) the

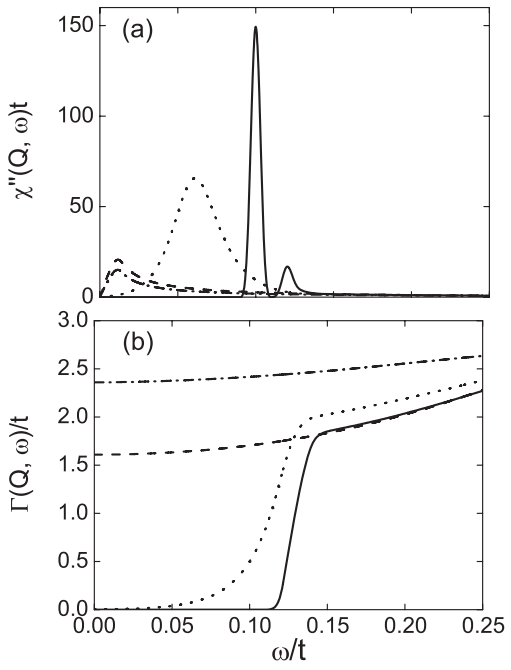

FIG. 5. (a) Spectral function $\chi''(\mathbf{Q},\omega)$ and (b) spin-excitation damping $\Gamma(\mathbf{Q},\omega)$ calculated in the particle-hole bubble approximation, Eq. (19), at $\delta = 0.2$ for the d-wave pairing ($\Delta_0 = 0.1t$ taken from Ref. 38) at $T = 0$ (solid line) and $T = 0.4T_c$ (dotted line), and for the normal state at $T = 0$ (dashed line) and $T = T_c$ (dash-dotted line).

spin excitation with the energy ω at the wave vector $\mathbf{Q}$ can decay only into a particle-hole pair with the energy $\omega(\mathbf{Q}) = E_{\mathbf{Q}+\mathbf{q}} + E_{\mathbf{q}}$, in the more general process described by Eq. (25) an additional spin excitation participates in the scattering. In the limit $T \to 0$, the decay process is governed by another energy-conservation law, $\omega(\mathbf{Q}) = E_{\mathbf{q}_3} + E_{\mathbf{q}_1} + \widetilde{\omega}_{\mathbf{q}_2}$, where the largest contribution from the spin excitation comes from $\widetilde{\omega}_{\mathbf{q}_2} \simeq \widetilde{\omega}_{\mathbf{Q}}$ due to the factor $m(\mathbf{q}_2)$, Eq. (14), in Eq. (25). This energy-momentum conservation law strongly reduces the phase space for the decay and suppresses the damping of the initial spin excitation with energy $\omega(\mathbf{Q})$. In fact, the occurrence of an additional spin excitation in the scattering process with the finite energy $\widetilde{\omega}_{\mathbf{Q}}$ plays a role similar to the superconducting gap in the excitation of the particle-hole pair in Eq. (26). Therefore, the damping at low temperatures ($k_B T \ll \widetilde{\omega}_{\mathbf{Q}} \sim E_r$) appears to be small even in the normal state as demonstrated in Fig. 1(c). In the case of particle-hole relaxation, the condition for the occurrence of the RM, $\omega(\mathbf{Q}) = E_{\mathbf{q}+\mathbf{Q}} + E_{\mathbf{q}} \leqslant 2\Delta(\mathbf{q}^*)$, imposes a strong restriction on the shape of the FS, which should cross the AF Brillouin zone to accommodate the scattering vector $\mathbf{Q}$ and the vector $\mathbf{q}^*$ on the FS. In the case of the full self-energy, Eq. (25), the energy-momentum conservation law for three quasiparticles does not impose such strong limitations.

C. Resonance mode

Experimentally, the RM energy E_r decreases with underdoping following the superconducting transition temperature, $E_r \simeq 5.3 k_B T_c$, but only weakly depends on temperature (see, e.g., Refs. 2 and 4). Now we discuss the temperature and doping dependence of the RM and its dispersion within our theory for the d-wave pairing.

The temperature dependence of the spectral function in the overdoped case $\delta = 0.2$ is shown in Fig. 6. It has high intensity at low temperatures, but strongly decreases with temperature and becomes very broad at $T \sim T_c$ as found in experiments (see Ref. 1). In Fig. 7 the temperature dependence of the spectral function for the underdoped case $\delta = 0.09$ is plotted. Whereas the resonance energy decreases with underdoping, the intensity of the RM greatly increases in accordance with experiments. The RM energy weakly depends on temperature and is still quite visible at $T = T_c$ and even at $T = 1.4T_c$.

The dispersion of the spectral function for $\delta = 0.2$ is shown in Figs. 8 and 9. A strong suppression of the spectral-function intensity away from $\mathbf{Q} = \pi(1,1)$ even at $T = 0$ explains the resonance-type behavior of the function at low temperatures. This suppression of the intensity is in accord with the sharp increase of the damping away from $\mathbf{Q}$ shown in Fig. 3. As can be seen from Figs. 8 and 9, we obtain an upward dispersion of the resonance energy $\Omega(\mathbf{Q}+\mathbf{q})$. Our numerical results may be well fitted by the quadratic dispersion law for small wave vectors, $(q_x, q_y) \lesssim 0.2\pi$,

$$\Omega(\mathbf{Q}+\mathbf{q}) = \left[E_{\mathbf{r}}^2 + c^2\left(q_x^2 + q_y^2\right)\right]^{1/2}, \tag{27}$$

where $E_{\mathbf{r}}/t = 0.12$ (0.09) and $c/at = 0.36$ (0.45) for $\delta = 0.2$ (0.09). In the conventional units we obtain $E_{\mathbf{r}} = 38$ meV, $c = 425$ meV Å for $\delta = 0.2$ and $E_{\mathbf{r}} = 28$ meV, $c = 545$ meV Å for $\delta = 0.09$, where we take $a = 3.82$ Å and $t = 313$ meV. Note that the quadratic dispersion was reported

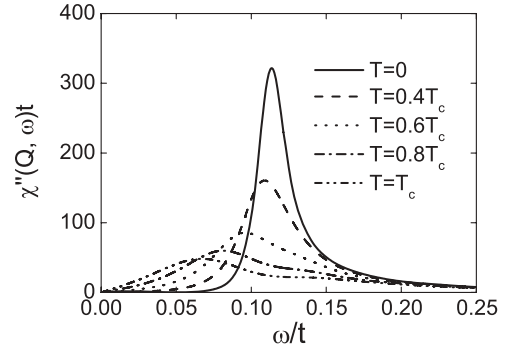

FIG. 6. Temperature dependence of the spectral function $\chi''(\mathbf{Q},\omega)$ at $\delta = 0.2$.

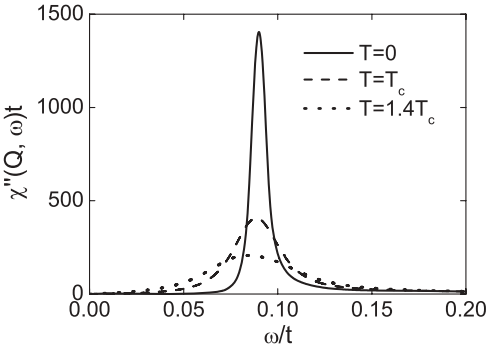

FIG. 7. Temperature dependence of the spectral function $\chi''(\mathbf{Q},\omega)$ at $\delta = 0.09$.

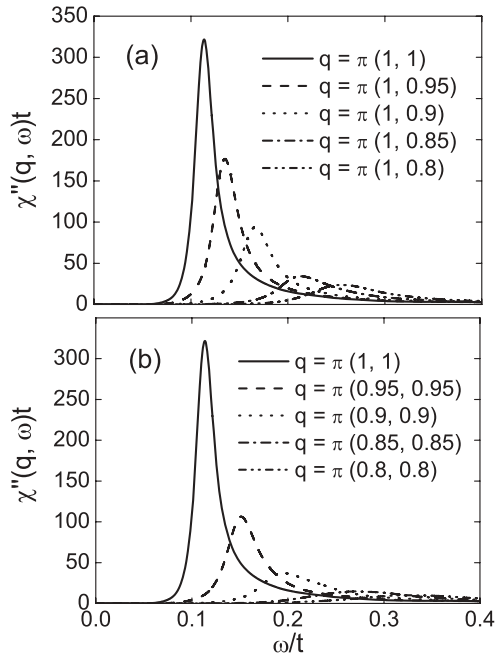

FIG. 8. Spectral function $\chi''(\mathbf{q},\omega)$ for the wave vectors (a) $\mathbf{q} = \pi(1,\xi)$ and (b) $\mathbf{q} = \pi(\xi,\xi)$ at $T = 0$ for $\delta = 0.2$.

in several papers. For example, the dispersion (27) was found in Ref. 15 for the acoustic mode in $YBCO_{6.5}$ ($\delta = 0.09$) with the parameters $E_{\mathbf{r}} = 33$ meV and $c \simeq 360$ meV Å which qualitatively agrees with our results.

We have not found the downward dispersion at energies below the RM detected in neutron-scattering experiments, for example, on $YBCO_{6.5}$ (Ref. 15) and on $YBCO_{6.6}$ (Refs. 16 and 17). However, as argued in Ref. 15, two distinct regions of spin excitations may be suggested: a low-energy part below $E_{\mathrm{r}} \approx 33$ meV, which can be described as incommensurate stripelike collective spin excitations for the acoustic mode, and a high-energy part, which has a spin-wave character. The high-energy part of the spin excitations has an isotropic in-plane dispersion while the low-energy excitations show a one-dimensional character. The different nature of the two parts of the spectrum is also revealed in their temperature dependence: the low-energy acoustic part of the spectrum is strongly influenced by the superconducting transition,

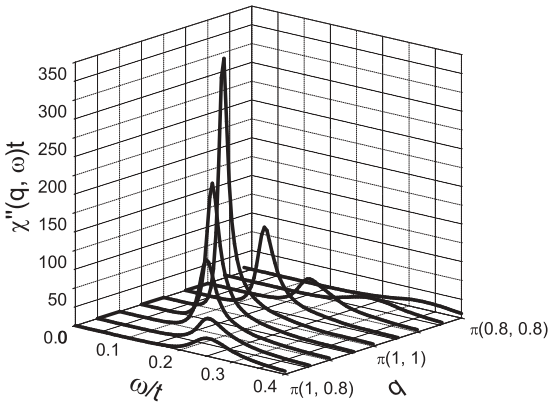

FIG. 9. Spectral function $\chi''(\mathbf{q},\omega)$ near the wave vector $\mathbf{Q} = \pi(1,1)$ at $T = 0$ for $\delta = 0.2$.

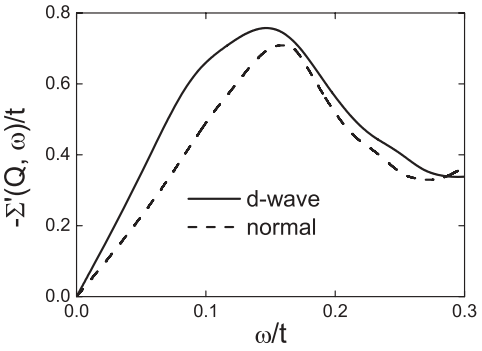

FIG. 10. Real part of the self-energy $\Sigma'(\mathbf{Q},\omega)$ for the d-wave pairing in comparison with the normal state at $T = 0$ for $\delta = 0.2$.

while the high-energy part of the spectrum does not change appreciably with temperature up to 85 K. Similar differences between the upward and downward dispersions were found in Refs. 16 and 17.

The downward dispersion of the lower-energy part of the spectrum was explained within the stripelike models, as discussed in the Introduction. It was also found for a Fermi-liquid model in the RPA approach (see, e.g., Ref. 24) or, for the t-J model, within the particle-hole bubble approximation (see Refs. 36,40,42). The dispersion was explained by a special wave-vector dependence of the particle-hole bubble diagram related to the wave-vector dependence of the $d_{x^2-y^2}$ superconducting gap and to a 2D FS that is specific to cuprates. Since in our theory beyond the RPA the RM energy does not critically depend on specific properties of the FS and the superconducting gap, the downward dispersion cannot be found. To discuss this problem in detail, the role of stripe excitations in the spin-excitation spectrum should be elucidated.

Now we discuss the doping dependence of the RM energy $E_{\mathrm{r}}(\delta)$. At low temperatures, the real part of the self-energy $\Sigma'(\mathbf{Q},\omega) < 0$ is quite large as shown in Fig. 10. This considerably softens the energy of spin excitations $\omega_{\mathbf{Q}}$ in the GMFA, Eq. (10), shifting the pole of the spectral function $\chi''(\mathbf{Q},\omega)$ to a lower energy: $\widetilde{\omega}_{\mathbf{Q}} = [\omega^2_{\mathbf{Q}} - \widetilde{\omega}_{\mathbf{Q}}\,|\Sigma'(\mathbf{Q},\widetilde{\omega}_{\mathbf{Q}})|]^{1/2}$. Experimentally, the RM energy is measured by the position E_{r} of the maximum in the spectral function $\chi''(\mathbf{Q},\omega)$ which deviates from $\widetilde{\omega}_{\mathbf{Q}}$ due to the finite width of the excitations. In Fig. 11 the doping dependence $E_{\mathrm{r}}(\delta)$ in the superconducting state at $T = 0$ determined by the maximum of the spectral function is plotted. Thereby, for the doping dependence of $\Delta_0(\delta) = 1.76\,T_{\mathrm{c}}(\delta)$ we used the universal empirical formula $T_{\mathrm{c}}(\delta) = T_{\mathrm{c,max}}\,[1 - \beta\,(\delta - \delta_{\mathrm{opt}})^2]$,[62] where $\delta_{\mathrm{opt}} = 0.16$, $T_{\mathrm{c,max}} = 93$ K, and the value of $\beta = 75$ was fitted to obtain $T_{\mathrm{c}} = 59$ K for $\delta = 0.09$ in $YBCO_{6.5}$.[14] With decreasing δ, E_{r} decreases, which qualitatively agrees with the experimental data. The energy of the RM tends to zero at the critical doping $\delta_{\mathrm{c}} = 0.038$, below which the long-range AF order emerges at $T = 0$, as we have shown in Ref. 45. So, in our scenario the RM is just the soft mode which brings about the long-range AF order below the critical doping.

Experimentally, in the overdoped region the RM energy decreases with increasing doping (see Fig. 11 and, e.g., Ref. 31), while in our theory E_{r} tends to increase due to

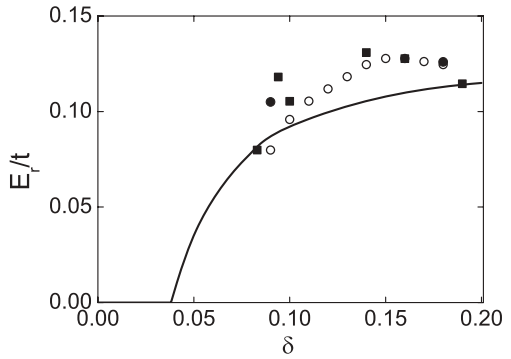

FIG. 11. Energy of the resonance mode E_r at $T = 0$ as a function of hole doping δ in comparison with experimental data for YBCO from Ref. 2 (open circles), Ref. 4 (full squares), and Refs. 1 and 14 (full circles).

the increasing energy $\widetilde{\omega}_{\mathbf{Q}}$. The agreement with experiments in Fig. 11 can be improved in the optimally doped region, $\delta \lesssim 0.2$, if we change the parameter t to $t = 0.4$ eV instead of the adopted value $t = 0.313$ eV. We also note that in the approach of Ref. 38 a too large superconducting gap $\Delta_0 \sim 0.1t$ (in comparison with our value $\Delta_0 \sim 0.044t$) has to be taken to fit the RM energy to the experimentally observed one.

In Fig. 12 we compare our results with the neutron-scattering data for the nearly optimally doped $YBCO_{6.92}$ single crystal[1] at $T = 5$ and 100 K. In this sample, $T_c = 91$ K and the RM energy $E_r \simeq 40$ meV$= 5.1 k_B T_c > 2\,\Delta_0$ [taking $2\Delta_0(\delta) = 3.52\, k_B T_c(\delta)$ we have $E_r \simeq 2.9\Delta_0$]. For $\delta = 0.2$, our calculations yield $E_r = 0.12t = 38$ meV$= 4.8 k_B T_c = 2.7\Delta_0$ ($t = 0.313$ eV, $k_B T_c = 0.025t$; see Sec. III A). Concerning the heights of the peaks, the scale of the experimental data, given in arbitrary units, was adjusted by fitting only the peak height at $T = 5$ K to our result at the same temperature.

In Fig. 13 our results are compared with the experimental data for the underdoped ortho-II $YBCO_{6.5}$ single crystal with $E_r = 33$ meV$= 6.5\, k_B T_c = 3.7\Delta_0$ at $T = 8$ and 85 K (see Fig. 14 in Ref. 14). For $\delta = 0.09$, our theory gives $E_r = 0.09t = 28$ meV$= 5.6\, k_B T_c = 3.2\Delta_0$. Here, the experimental peak heights were also scaled by fitting only the peak height at $T = 8$ K to our result at the same temperature. We note a weak temperature dependence of the RM energy observed experimentally and obtained in our calculation. In both

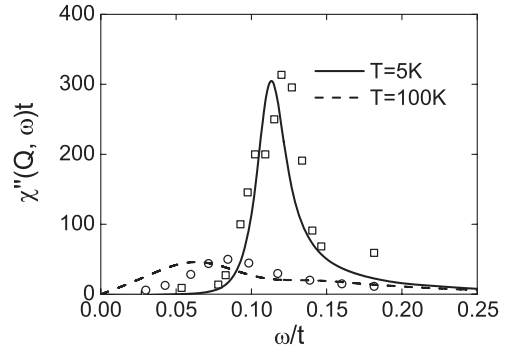

FIG. 12. Spectral function $\chi''(\mathbf{Q},\omega)$ for doping $\delta = 0.2$ compared to experimental data for $YBCO_{6.92}$, Ref. 1, at $T = 5$ K (squares) and $T = 100$ K (circles).

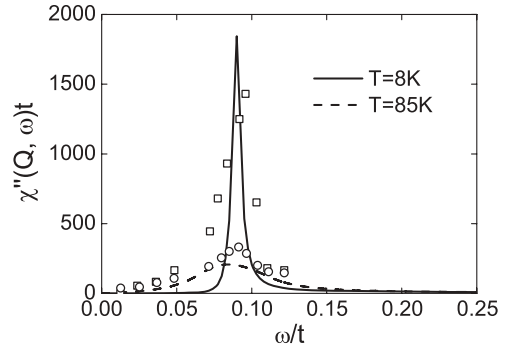

FIG. 13. Spectral function $\chi''(\mathbf{Q},\omega)$ for doping $\delta = 0.09$ compared to experimental data for $YBCO_{6.5}$, Ref. 14, at $T = 8$ K (squares) and $T = 85$ K (circles).

compounds the RM energy is larger than the superconducting excitation energy, $2\Delta_0$, while in the spin-1 exciton scenario the RM energy E_r has to be less than $2\Delta_0$. So we obtain a good agreement of our theory with neutron-scattering experiments on YBCO crystals both near the optimal doping and in the underdoped region.

It is also interesting to compare our results with the recent detailed experimental study of the spin-excitation spectrum reported in Refs. 16 and 17 for the twin-free $YBCO_{6.6}$ crystal with $T_c = 61$ K at hole doping $\delta = 0.12$. For that, we calculate the spectral function $\chi''(\mathbf{q},\omega)$ for the same hole doping and

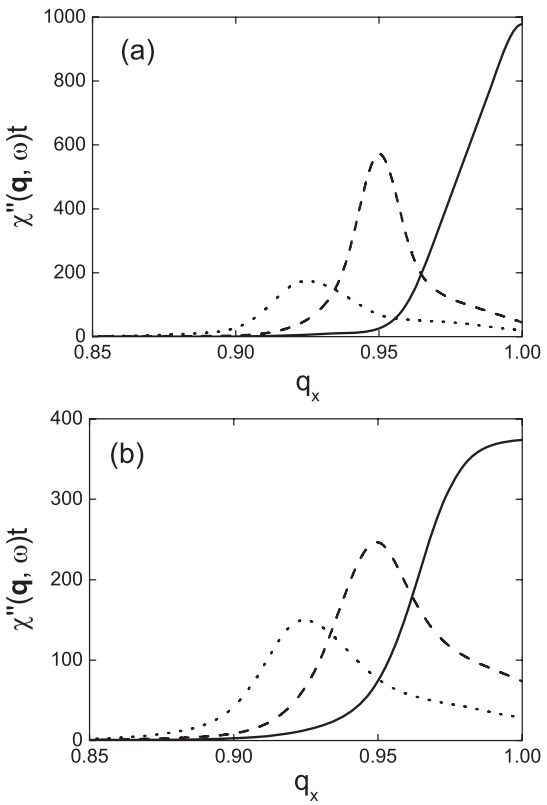

FIG. 14. Spectral function $\chi''(\mathbf{q},\omega)$ for $\mathbf{q} = \pi(q_x, 1)$ at doping $\delta = 0.12$ and energies $\omega/E_r = 1$ (bold line), 1.24 (dashed line), and 1.58 (dotted line) at (a) $T = 0$ and (b) $T = 70$ K (in units of $t = 0.4$ eV).

T_c. From the experimental value $\omega_r = 38$ meV and damping $\Gamma = 11$ meV we calculate $E_r = 36.4$ meV.[63] To get agreement with the theoretical value $E_r = 0.091t$ we adopt $t = 0.4$ eV, as also inferred from the angle-resolved photoemission spectroscopy data in $YBCO_{6.6}$.[18] For the upper branch of spin excitations above the RM we obtain a quadratic dispersion given by Eq. (27), whereas in Ref. 17, Eq. (11), the dispersion was fitted by a quartic power law.

For a more detailed comparison of the RM dispersion with the experimental data in Ref. 17 for the upper branch, in Fig. 14 we present the spectral function $\chi''(\mathbf{q},\omega)$ at $T = 0$ and $T = 70$ K for the wave vectors $\mathbf{q} = \pi(q_x,1)$ at energies $\omega/E_r = 1$, 1.24, and 1.58 which, putting $E_r = \omega_r$, corresponds to $\omega = 38$, 47, and 60 meV in Ref. 17. The damping of the RM in our theory strongly depends on $\mathbf{q}$ as shown in Fig. 3, whereas in Ref. 17 the damping was taken to be q independent, $\Gamma = 11$ meV. In our calculations we get a much smaller damping: $\Gamma_{\mathbf{Q}} = 0.0034t \simeq 1.4$ meV at $T = 0$. These differences result in much sharper spectral functions in our theory in comparison with the experimental data.[17] In particular, the half width at half maximum at $\mathbf{q} = \mathbf{Q} = \pi(1,1)$ equals $\Delta q = 0.021\pi$ in Fig. 14(a) and $\Delta q = 0.038\pi$ in Fig. 14(b), in comparison with the values $\Delta q \approx 0.2\pi$ at $T = 5$ K and $\Delta q \approx 0.24\pi$ at $T = 70$ K in Fig. 3 of Ref. 17, which are about 7–8 times larger than our results. We believe that the difference in the damping may be explained by impurity scattering due to a disorder in the chains in the $YBCO_{6.6}$ sample or by an inhomogeneity produced by dynamical stripe fluctuations. The latter may be also the reason that we have not found a change of the dispersion topology above T_c as observed in Ref. 17, which was related to the appearance of an electronic liquid-crystal state.

IV. CONCLUSION

A detailed study of the DSS in the superconducting state has revealed the important role of the spin-excitation damping in the RM phenomenon. We have found that the low-temperature damping essentially depends on the gap $\widetilde{\omega}_{\mathbf{Q}} \simeq E_r$ in the spin-excitation spectrum at the AF wave vector $\mathbf{Q}$, while the opening of a superconducting gap $2\Delta(T)$ below T_c is less important. Since the energy of the RM $E_r \sim 5\,k_B T_c$ does not show temperature dependence, at $T \lesssim T_c$, the spin gap at E_r plays the dominant role in the suppression of damping, since the superconducting energy $2\Delta(T \lesssim T_c) \ll E_r$. This follows from Eq. (25) for the self-energy, where in the decay of a spin excitation, besides a particle-hole pair, the contribution from an additional spin excitation is taken into account. This is in contrast to the particle-hole bubble approximation in Eq. (26) which is used in the RPA (see, e.g., Refs. 24,36) and in similar approximations in memory-function theories.[38,40,42] In those approximations, the spin-excitation damping is much larger in the normal state and reveals a spin gap only at $T \ll T_c$, where the RM appears (see Fig. 5). The gapped spin-excitation spectrum in the full self-energy (25) greatly suppresses the damping at $T = 0$, which results in a comparable damping both in the superconducting state (either of d-wave or s-wave symmetry) and in the normal state, as demonstrated in Figs. 1 and 3. The damping is strongly decreasing in the underdoped region (see Figs. 2 and 3), bringing about a much stronger RM seen also above T_c (Fig. 7).

The weak temperature dependence of the RM in cuprates can be contrasted with the magnetic RM in iron arsenide superconductors. In particular, a perfect scaling of the RM energy with the superconducting gap below $T_c = 25$ K observed in the $BaFe_{1.85}Co_{0.15}As_2$ crystal[64] supports the spin-1 exciton scenario expected in AF metals where the SDW instability determines the spin-excitation spectrum. In contrast to iron arsenides, strong electron correlations in cuprates lead to a large AF exchange interaction between localized copper spins that results in temperature-independent spin-wave-like excitations. A scenario of preformed Cooper pairs in cuprates, which may also explain a weak RM temperature dependence, seems to contradict experiments (for discussions, see Ref. 5).

With decreasing hole concentration the energy of the RM decreases and shows a dependence close to that observed in neutron-scattering experiments, $E_r \sim 5k_B T_c$ (see Fig. 11). Due to the important role of gapped spin excitations in the damping of the RM, its energy E_r does not critically depend on the superconducting gap energy $2\Delta(T)$ and hence on temperature and peculiarities of the electronic spectrum in cuprates, contrary to the theories based on the RPA (see, e.g., Refs. 24 and 36). In particular, E_r is found to be larger than $2\Delta_0$ as observed in experiments (see Figs. 12 and 13).

It should be stressed that the damping of the RM in our microscopic theory within the t-J model is determined by the kinematical interaction induced by the kinetic energy t of electrons moving in a singly occupied Hubbard subband. This interaction is absent in conventional fermion models in which strong electron correlations are neglected and the spin-electron scattering is determined by a phenomenological interaction with a coupling constant as a fit parameter.

Finally, let us note that our approach, using the MFA for the electronic spectral functions, Eqs. (22) and (23), in the computation of the self-energy (25), has to be considered as a first step toward a fully self-consistent theory of the DSS in the t-J model. However, we believe that the consideration of more accurate fermionic GFs in Eqs. (16) and (17) beyond the Hubbard-I approximation (see, e.g., Ref. 65) should not change our main conclusions, since the electron dispersion, as shown in Fig. 2, does not play an essential role in our theory in contrast to the spin-exciton scenario.

ACKNOWLEDGMENTS

We thank V. Hinkov for fruitful discussions. Partial financial support by the Heisenberg–Landau Program of JINR is acknowledged. One of the authors (N.P.) is grateful to the MPIPKS, Dresden, for the hospitality during his stay at the Institute, where a part of the present work has been done.

APPENDIX: MODE-COUPLING APPROXIMATION

To calculate the self-energy (4) we use the MCA for the time-dependent multiparticle correlation function which appears in the spectral representation of the relaxation function

$$\Sigma''(\mathbf{q},\omega) = -\frac{1}{2\omega\, m(\mathbf{q})}[I(\mathbf{q},-\omega) - I(\mathbf{q},\omega)],$$
$$I(\mathbf{q},\omega) = \int_{-\infty}^{\infty} dt\, e^{i\omega t} \langle \ddot{S}^-_{\mathbf{q}} | \ddot{S}^+_{-\mathbf{q}}(t) \rangle^{\text{proper}}, \tag{A1}$$

where

$$-\ddot{S}_i^+ = [[S_i^+,(H_t+H_J)],(H_t+H_J)] \equiv \sum_\alpha F_i^\alpha \quad \text{(A2)}$$

determines the force correlation functions of the force operators F_i^α denoted by the index $\alpha = tt, tJ, Jt, JJ$. As discussed in Ref. 45, at the sizable doping $\delta \sim 0.1$ considered in this paper, only the term F_i^{tt} can be taken into account, since all other terms give negligible contributions. For this term we have

$$F_i^{tt} = \sum_{j,n} t_{ij}\{t_{jn}[H_{ijn}^- + H_{nji}^+] - t_{in}[H_{jin}^- + H_{nij}^+]\},$$
$$H_{ijn}^\sigma = X_i^{\sigma 0} X_j^{+-} X_n^{0\sigma} + X_i^{+0}\left(X_j^{00} + X_j^{\sigma\sigma}\right) X_n^{0-}. \quad \text{(A3)}$$

Following the reasoning of Ref. 45, in Eq. (A3) only products of operators on different sites are taken into account. After Fourier transformation to the $\mathbf{q}$ space we obtain the force-force correlation function

$$\left\langle \left[F_{\mathbf{q}}^{tt}\right]^\dagger \middle| F_{\mathbf{q}}^{tt}(t)\right\rangle = (2t)^4 \sum_{\mathbf{q}_1,\mathbf{q}_2} \sum_{\mathbf{q}_1',\mathbf{q}_2'} \left\langle \left[\Lambda_{\mathbf{q}_1',\mathbf{q}_2',\mathbf{q}_3'} H_{\mathbf{q}_1',\mathbf{q}_2',\mathbf{q}_3'}^- + \Lambda_{\mathbf{q}_3',\mathbf{q}_2',\mathbf{q}_1'} H_{\mathbf{q}_1',\mathbf{q}_2',\mathbf{q}_3'}^+\right]^\dagger \middle| [\Lambda_{\mathbf{q}_1,\mathbf{q}_2,\mathbf{q}_3} H_{\mathbf{q}_1,\mathbf{q}_2,\mathbf{q}_3}^-(t) + \Lambda_{\mathbf{q}_3,\mathbf{q}_2,\mathbf{q}_1} H_{\mathbf{q}_1,\mathbf{q}_2,\mathbf{q}_3}^+(t)]\right\rangle, \quad \text{(A4)}$$

where $\mathbf{q}_3 = \mathbf{q} - \mathbf{q}_1 - \mathbf{q}_2$ and $\mathbf{q}'_3 = \mathbf{q} - \mathbf{q}'_1 - \mathbf{q}'_2$. Here we introduce the vertex function

$$\Lambda_{\mathbf{q}_1\mathbf{q}_2\mathbf{q}_3} = 4(\gamma_{\mathbf{q}_3+\mathbf{q}_2} - \gamma_{\mathbf{q}_1})\gamma_{q_3} + \gamma_{\mathbf{q}_2} - \gamma_{\mathbf{q}_1+\mathbf{q}_3}, \quad \text{(A5)}$$

where the terms linear in $\gamma_{\mathbf{q}}$ reflect the exclusion of terms in F_i^{tt} with coinciding sites.

In the MCA we assume that the propagation of electronic- and bosonic-type excitations at different lattice sites in Eq. (A3) occurs independently, which results in the decoupling of the correlation function (A4) into the corresponding single-particle time-dependent correlation functions. As it turned out by numerical evaluations (see also Ref. 45), the contribution from the charge excitations given by $(X_j^{00} + X_j^{\sigma\sigma})$ in Eq. (A3) can be neglected in comparison with the spin-excitation contribution given by $X_j^{+-} = S_j^+$. In this approximation we obtain the spin-diagonal correlation functions for the normal state

$$\left\langle \left[H_{\mathbf{q}_1',\mathbf{q}_2',\mathbf{q}_3'}^\sigma\right]^\dagger \middle| H_{\mathbf{q}_1,\mathbf{q}_2,\mathbf{q}_3}^\sigma(t)\right\rangle = \left\langle X_{\mathbf{q}_3'}^{\sigma 0} S_{-\mathbf{q}_2'}^- X_{\mathbf{q}_1'}^{0\sigma} \middle| X_{\mathbf{q}_1}^{\sigma 0}(t) S_{\mathbf{q}_2}^+(t) X_{\mathbf{q}_3}^{0\sigma}(t)\right\rangle = \left\langle X_{\mathbf{q}_1}^{0\sigma} X_{\mathbf{q}_1}^{\sigma 0}(t)\right\rangle \left\langle S_{-\mathbf{q}_2}^- S_{\mathbf{q}_2}^+(t)\right\rangle \left\langle X_{\mathbf{q}_3}^{\sigma 0} X_{\mathbf{q}_3}^{0\sigma}(t)\right\rangle \times \delta_{\mathbf{q}_1,\mathbf{q}_1'}\delta_{\mathbf{q}_2,\mathbf{q}_2'}\delta_{\mathbf{q}_3,\mathbf{q}_3'}. \quad \text{(A6)}$$

In the superconducting state we additionally take into account pair correlation functions which appear in the spin off-diagonal terms,

$$\left\langle \left[H_{\mathbf{q}_1',\mathbf{q}_2',\mathbf{q}_3'}^{\bar\sigma}\right]^\dagger \middle| H_{\mathbf{q}_1,\mathbf{q}_2,\mathbf{q}_3}^\sigma(t)\right\rangle = \left\langle X_{\mathbf{q}_3'}^{\bar\sigma 0} S_{-\mathbf{q}_2'}^- X_{\mathbf{q}_1'}^{0\bar\sigma} \middle| X_{\mathbf{q}_1}^{\sigma 0}(t) S_{\mathbf{q}_2}^+(t) X_{\mathbf{q}_3}^{0\sigma}(t)\right\rangle = -\left\langle X_{-\mathbf{q}_3}^{0\bar\sigma} X_{\mathbf{q}_3}^{0\sigma}(t)\right\rangle \left\langle S_{-\mathbf{q}_2}^- S_{\mathbf{q}_2}^+(t)\right\rangle \left\langle X_{-\mathbf{q}_1}^{\bar\sigma 0} X_{\mathbf{q}_1}^{\sigma 0}(t)\right\rangle \times \delta_{\mathbf{q}_1,-\mathbf{q}_3'}\delta_{\mathbf{q}_2,\mathbf{q}_2'}\delta_{\mathbf{q}_3,-\mathbf{q}_1'}. \quad \text{(A7)}$$

By substituting the MCA correlation functions (A6) and (A7) in Eq. (A1) we obtain the multiparticle correlation function

$$I(\mathbf{q},\omega) = \int_{-\infty}^{\infty} dt e^{i\omega t} \frac{1}{N^2} \sum_{\mathbf{q}_1,\mathbf{q}_2} \langle S_{-\mathbf{q}_2}^- S_{\mathbf{q}_2}^+(t)\rangle \times \left[\left(\Lambda_{\mathbf{q}_1,\mathbf{q}_2,\mathbf{q}_3}^2 + \Lambda_{\mathbf{q}_3,\mathbf{q}_2,\mathbf{q}_1}^2\right)\left\langle X_{\mathbf{q}_1}^{0\sigma} X_{\mathbf{q}_1}^{\sigma 0}(t)\right\rangle\left\langle X_{\mathbf{q}_3}^{\sigma 0} X_{\mathbf{q}_3}^{0\sigma}(t)\right\rangle - \Lambda_{\mathbf{q}_1,\mathbf{q}_2,\mathbf{q}_3}\Lambda_{\mathbf{q}_3,\mathbf{q}_2,\mathbf{q}_1} \sum_\sigma \left\langle X_{-\mathbf{q}_1}^{\bar\sigma 0} X_{\mathbf{q}_1}^{\sigma 0}(t)\right\rangle\left\langle X_{-\mathbf{q}_3}^{0\bar\sigma} X_{\mathbf{q}_3}^{0\sigma}(t)\right\rangle\right]. \quad \text{(A8)}$$

Using the spectral representation for the time-dependent correlation functions (see, e.g., Ref. 59)

$$\langle BA(t)\rangle = \int_{-\infty}^{\infty} d\omega\, e^{-i\omega t} f(\omega)[-(1/\pi)]\mathrm{Im}\langle\langle A|B\rangle\rangle_\omega, \quad \text{(A9)}$$

where $f(\omega)$ is the Fermi (Bose) function $n(\omega)$ $[N(\omega)]$, after integration over time t we derive Eq. (15).

[1] Ph. Bourges, in *The Gap Symmetry and Fluctuations in High Temperature Superconductors*, edited by J. Bok, G. Deutscher, D. Pavuna, and S. A. Wolf, NATO Advanced Studies Institute, Series B: Physics (Plenum Press, New York, 1998), Vol. 371, pp. 349–371.

[2] Y. Sidis, S. Pailhès, B. Keimer, Ph. Bourges, C. Ulrich, and L. P. Regnault, Phys. Status Solidi B **241**, 1204 (2004).

[3] Y. Sidis, S. Pailhès, V. Hinkov, B. Fauqué, C. Ulrich, L. Capogna, A. Ivanov, L.-P. Regnault, B. Keimer, and P. Bourges, C. R. Phys. **8**, 745 (2007).

[4] M. Eschrig, Adv. Phys. **55**, 47 (2006).

[5] N. M. Plakida, *High Temperature Cuprate Superconductors*, (Springer, Berlin, 2010), pp. 51–99.

[6] Q. Si, Y. Zha, K. Levin, and J. P. Lu, Phys. Rev. B **47**, 9055 (1993).

[7] H. F. Fong, Ph. Bourges, Y. Sidis, L. P. Regnault, J. Bossy, A. Ivanov, D. L. Milius, I. A. Aksay, and B. Keimer, Phys. Rev. B **61**, 14773 (2000).

[8] P. Dai, H. A. Mook, R. D. Hunt, and F. Doğan, Phys. Rev. B **63**, 054525 (2001).

[9] H. Yamase and W. Metzner, Phys. Rev. B **73**, 214517 (2006).

[10] J. Rossat-Mignod, L. P. Regnault, C. Vettier, P. Bourges, P. Burlet, J. Bossy, J. Y. Henry, and G. Lapertot, Physica C **185-189**, 86 (1991).

[11] H. He, P. Bourges, Y. Sidis, C. Ulrich, L. P. Regnault, S. Pailhès, N. S. Berzigiarova, N. N. Kolesnikov, and B. Keimer, Science **295**, 1045 (2002).

[12] G. Yu, Y. Li, E. M. Motoyama, X. Zhao, N. Barisic, Y. Cho, P. Bourges, K. Hradil, R. A. Mole, and M. Greven, Phys. Rev. B **81**, 064518 (2010).

[13] S. D. Wilson, P. Dai1, S. Li, S. Chi, H. J. Kang, and J. W. Lynn, Nature (London) **442**, 59 (2006).

[14] C. Stock, W. J. L. Buyers, R. Liang, D. Peets, Z. Tun, D. Bonn, W. N. Hardy, and R. J. Birgeneau, Phys. Rev. B **69**, 014502 (2004).

[15]C. Stock, W. J. L. Buyers, R. A. Cowley, P. S. Clegg, R. Coldea, C. D. Frost, R. Liang, D. Peets, D. Bonn, W. N. Hardy, and R. J. Birgeneau, Phys. Rev. B **71**, 024522 (2005).
[16]V. Hinkov, Ph. Bourges, S. Pailhès, Y. Sidis, A. Ivanov, C. D. Frost, T. G. Perring, C. T. Lin, D. P. Chen, and B. Keimer, Nature Phys. **3**, 780 (2007).
[17]V. Hinkov, B. Keimer, A. Ivanov, Ph. Bourges, Y. Sidis, and C. D. Frost, e-print arXiv:1006.3278 [cond-mat].
[18]T. Dahm, V. Hinkov, S. V. Borisenko, A. A. Kordyuk, V. B. Zabolotnyy, J. Fink, B. Büchner, D. J. Scalapino, W. Hanke, and B. Keimer, Nature Phys. **5**, 217 (2009).
[19]N. B. Christensen, D. F. McMorrow, H. M. Rønnow, B. Lake, S. M. Hayden, G. Aeppli, T. G. Perring, M. Mangkorntong, M. Nohara, and H. Takagi, Phys. Rev. Lett. **93**, 147002 (2004).
[20]B. Vignolle, S. M. Hayden, D. F. McMorrow, H. M. Rønnow, B. Lake, C. D. Frost, and T. G. Perring, Nature Phys. **3**, 163 (2007).
[21]O. J. Lipscombe, B. Vignolle, T. G. Perring, C. D. Frost, and S. M. Hayden, Phys. Rev. Lett. **102**, 167002 (2009).
[22]M. R. Norman, Phys. Rev. B **61**, 14751 (2000).
[23]D. Manske, I. Eremin, and K. H. Bennemann, Phys. Rev. B **63**, 054517 (2001).
[24]I. Eremin, D. K. Morr, A. V. Chubukov, K. Bennemann, and M. R. Norman, Phys. Rev. Lett. **94**, 147001 (2005).
[25]Q. Si, J. P. Lu, and K. Levin, Phys. Rev. B **45**, 4930 (1992).
[26]Y. Zha, K. Levin, and Q. Si, Phys. Rev. B **47**, 9124 (1993).
[27]D. Z. Liu, Y. Zha, and K. Levin, Phys. Rev. Lett. **75**, 4130 (1995).
[28]Y. J. Kao, Q. Si, and K. Levin, Phys. Rev. B **61**, R11898 (2000).
[29]I. Eremin, D. K. Morr, A. V. Chubukov, and K. Bennemann, Phys. Rev. B **75**, 184534 (2007).
[30]B. Fauqué, Y. Sidis, L. Capogna, A. Ivanov, K. Hradil, C. Ulrich, A. I. Rykov, B. Keimer, and P. Bourges, Phys. Rev. B **76**, 214512 (2007).
[31]S. Pailhés, C. Ulrich, B. Fauqué, V. Hinkov, Y. Sidis, A. Ivanov, C. T. Lin, B. Keimer, and P. Bourges, Phys. Rev. Lett. **96**, 257001 (2006).
[32]M. Ogata and H. Fukuyama, Rep. Prog. Phys. **71**, 036501 (2008).
[33]J. Brinckmann and P. A. Lee, Phys. Rev. B **65**, 014502 (2001).
[34]J. Hubbard, Proc. R. Soc. London, Ser. A **285**, 542 (1965).
[35]Yu. A. Izyumov and B. M. Letfulov, J. Phys. Condens. Matter **3**, 5373 (1991).
[36]F. Onufrieva and P. Pfeuty, Phys. Rev. B **65**, 054515 (2002).
[37]H. Mori, Prog. Theor. Phys. **34**, 399 (1965).
[38]I. Sega, P. Prelovšek, and J. Bonča, Phys. Rev. B **68**, 054524 (2003).
[39]P. Prelovšek, I. Sega, and J. Bonča, Phys. Rev. Lett. **92**, 027002 (2004).
[40]I. Sega and P. Prelovšek, Phys. Rev. B **73**, 092516 (2006).
[41]P. Prelovšek and I. Sega, Phys. Rev. B **74**, 214501 (2006).
[42]A. Sherman and M. Schreiber, Phys. Rev. B **68**, 094519 (2003).
[43]A. Sherman and M. Schreiber, Fiz. Nizk. Temp. (Low Temp. Phys., Ukraine) **32**, 499 (2006).
[44]A. A. Vladimirov, D. Ihle, and N. M. Plakida, Theor. Math. Phys. **145**, 1576 (2005).
[45]A. A. Vladimirov, D. Ihle, and N. M. Plakida, Phys. Rev. B **80**, 104425 (2009).
[46]R. Zeyher, Europhys. Lett. **90**, 17006 (2010).
[47]J. M. Tranquada, in *Handbook of High-Temperature Superconductivity. Theory and Experiment*, edited by J. R. Schrieffer and J. S. Brooks (Springer, New York, 2007), pp. 257–298.
[48]S. A. Kivelson, E. Fradkin, V. Oganesyan, I. P. Bindloss, J. M. Tranquada, A. Kapitulnik, and C. Howald, Rev. Mod. Phys. **75**, 1201 (2003).
[49]M. Vojta, Adv. Phys. **58**, 699 (2009).
[50]J. M. Tranquada, H. Woo, T. G. Perring, H. Goka, G. D. Gu1, G. Xu, M. Fujita, and K. Yamada, Nature (London) **429**, 534 (2004).
[51]M. Vojta and T. Ulbricht, Phys. Rev. Lett. **93**, 127002 (2004).
[52]G. S. Uhrig, K. P. Schmidt, and M. Grüninger, Phys. Rev. Lett. **93**, 267003 (2004).
[53]G. Seibold and J. Lorenzana, Phys. Rev. Lett. **94**, 107006 (2005).
[54]B. M. Andersen and P. Hedegärd, Phys. Rev. Lett. **95**, 037002 (2005).
[55]B. M. Andersen and O. F. Syljuåsen, Phys. Rev. B **75**, 012506 (2007).
[56]R. M. Konik, F. H. L. Essler, and A. M. Tsvelik, Phys. Rev. B **78**, 214509 (2008).
[57]V. Hinkov, S. Pailhès, Ph. Bourges, Y. Sidis, A. Ivanov, A. Kulakov, C. T. Lin, D. P. Chen, C. Bernhard, and B. Keimer, Nature (London) **430**, 650 (2004).
[58]H. A. Mook, P. Dai, F. Doğan, and R. D. Hunt, Nature (London) **404**, 729 (2000).
[59]D. N. Zubarev, Sov. Phys. Usp. **3**, 320 (1960).
[60]Yu. A. Tserkovnikov, Theor. Math. Phys. **49**, 993 (1981); **52**, 712 (1982).
[61]H. Won and K. Maki, Phys. Rev. B **49**, 1397 (1994).
[62]J. L. Tallon, C. Bernhard, H. Shaked, R. L. Hitterman, and J. D. Jorgensen, Phys. Rev. B **51**, 12911 (1995).
[63]The maximum of the DSS, Eq. (7), which defines the RM energy E_r, is given by the equation $E_r = (\omega_r/\sqrt{3})[1 - 2\gamma^2 + 2\sqrt{1-\gamma^2}]^{1/2}$, where $\gamma = \Gamma/\omega_r$ and, in our notation, $\omega_r = \widetilde{\omega}_{\mathbf{Q}}$ and $2\Gamma = -\Sigma''(\mathbf{Q},\widetilde{\omega}_{\mathbf{Q}})$.
[64]D. S. Inosov, J. T. Park, P. Bourges, D. L. Sun, Y. Sidis, A. Schneidewind, K. Hradil, D. Haug, C. T. Lin, B. Keimer, and V. Hinkov, Nature Phys. **6**, 178 (2010).
[65]N. M. Plakida and V. S. Oudovenko, J. Exp. Theor. Phys. **104**, 230 (2007).